BIOCHEMISTRY
including biophysical chemistry & molecular biology

Article

pubs.acs.org/biochemistry

Adenine Phosphoribosyltransferase from *Sulfolobus solfataricus* Is an Enzyme with Unusual Kinetic Properties and a Crystal Structure that Suggests It Evolved from a 6-Oxopurine Phosphoribosyltransferase

Kaj Frank Jensen,*[,†] Michael Riis Hansen,[†] Kristine Steen Jensen,[†,#] Stig Christoffersen,[‡] Jens-Christian Navarro Poulsen,[‡] Anne Mølgaard,[‡] and Anders Kadziola*[,‡]

[†]University of Copenhagen, Department of Biology, Ole Maaløes Vej 5, DK-2200 Copenhagen N, Denmark

[‡]University of Copenhagen, Department of Chemistry, Center of Crystallographic Studies, Universitetsparken 5, DK-2100 Copenhagen Ø, Denmark

Supporting Information

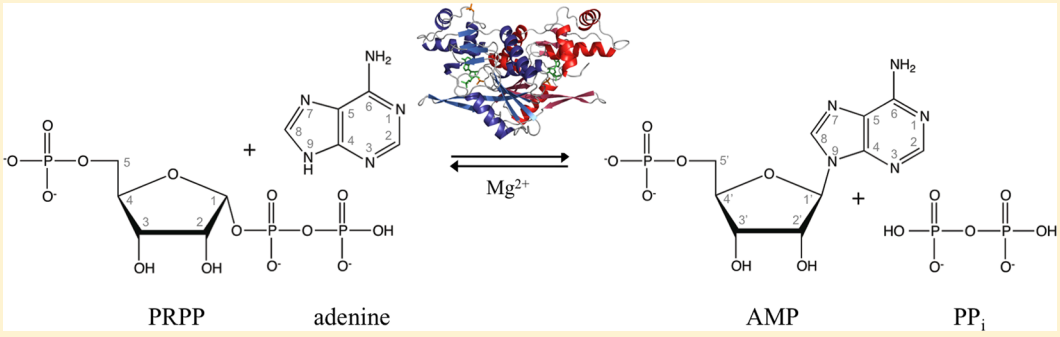

ABSTRACT: The adenine phosphoribosyltransferase (APRTase) encoded by the open reading frame SSO2342 of *Sulfolobus solfataricus* P2 was subjected to crystallographic, kinetic, and ligand binding analyses. The enzyme forms dimers in solution and in the crystals, and binds one molecule of the reactants 5-phosphoribosyl-α-1-pyrophosphate (PRPP) and adenine or the product adenosine monophosphate (AMP) or the inhibitor adenosine diphosphate (ADP) in each active site. The individual subunit adopts an overall structure that resembles a 6-oxopurine phosphoribosyltransferase (PRTase) more than known APRTases implying that APRT functionality in Crenarchaeotae has its evolutionary origin in this family of PRTases. Only the N-terminal two-thirds of the polypeptide chain folds as a traditional type I PRTase with a five-stranded β-sheet surrounded by helices. The C-terminal third adopts an unusual three-helix bundle structure that together with the nucleobase-binding loop undergoes a conformational change upon binding of adenine and phosphate resulting in a slight contraction of the active site. The inhibitor ADP binds like the product AMP with both the α- and β-phosphates occupying the 5′-phosphoribosyl binding site. The enzyme shows activity over a wide pH range, and the kinetic and ligand binding properties depend on both pH and the presence/absence of phosphate in the buffers. A slow hydrolysis of PRPP to ribose 5-phosphate and pyrophosphate, catalyzed by the enzyme, may be facilitated by elements in the C-terminal three-helix bundle part of the protein.

Adenine phosphoribosyltransferases (APRTases) catalyze Mg^{2+} dependent reactions between 5-phosphoribosyl-α-1-pyrophosphate (PRPP) and the nitrogenous base adenine leading to formation of adenosine monophosphate (AMP) and pyrophosphate (PP_i) (Scheme 1). Similar transferase reactions participate in the synthesis of other purine and pyrimidine nucleotides, the pyridine coenzymes (NAD and NADP), and the amino acids histidine and tryptophan.[1]

For the salvage of preformed purine bases, organisms generally contain one phosphoribosyltransferase (PRTase) specific for adenine and one or more PRTases with variant specificities toward the 6-oxopurine bases.[2] In the genome of the thermoacidophile archeon *Sulfolobus solfataricus* (*S. solfataricus*)[3] the open reading frame, SSO2424 (*gpT-2*) encodes a 6-oxopurine PRTase active with hypoxanthine, xanthine, and guanine as the purine base substrates, while the open reading frame SSO2342 (*gpT-1*) encodes an APRTase.[4,5] This communication is devoted to the characterization of the APRTase. Crystal structures and a kinetic characterization of the 6-oxopurine PRTase will be described elsewhere.

The type I PRTases are generally composed of a core consisting of a five-stranded β-sheet surrounded by helices, a hood structure involved in binding of the nucleobase substrate, and a flexible loop that covers the active site during catalysis. The active site is located in a cavity of the core part flanked by the hood and the flexible loop.[6−10] The bottom of the active site cavity contains an approximately 11-residue sequence

Received: October 26, 2014
Revised: March 13, 2015
Published: March 19, 2015

DOI: 10.1021/bi501334m
Biochemistry 2015, 54, 2323−2334

Scheme 1. Reaction Catalyzed by APRTase

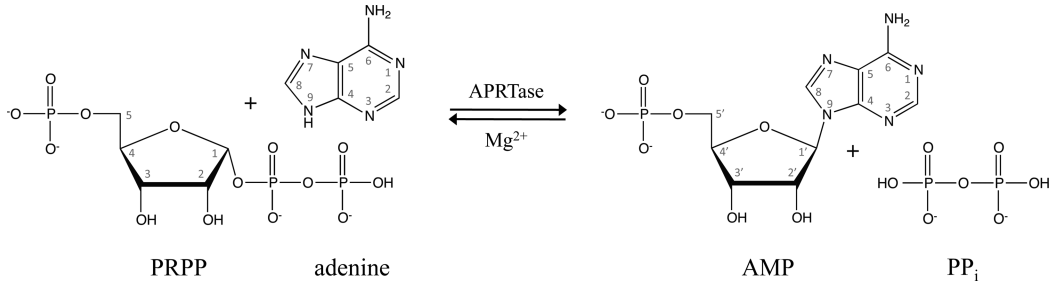

segment, termed the PRPP binding motif, which is found in PRPP synthetase and all type I PRTases. This sequence segment flanks the 5′-phosphoribosyl moiety of bound nucleotide products and PRPP and was originally thought to be the major determinant of PRPP binding.[11,12] However, recent studies of orotate PRTase have revealed that amino acid residues in the flexible loop also may be crucial for PRPP binding.[13]

The APRTase of *S. solfataricus* is unusual in several ways: First, the open reading frame (SSO2342) encoding this enzyme was originally annotated as a gene (*gpT-1*) encoding a 6-oxopurine PRTase due to a higher sequence similarity to known 6-oxopurine PRTases especially the *Escherichia coli* xanthine-guanine PRTase (XGPRTase) than to any known APRTase.[3,4] Second, the sequence of the PRPP binding motif[12,14] that generally correlates with the specificity of PRTases toward their nucleobase substrate[15] resembles that of the 6-oxopurine PRTases more than it resembles that of known APRTases. Third, only the N-terminal two-thirds of the sequence bears similarity to type I PRTases in general, while the C-terminal third of the protein bears no major resemblance to any known protein aside of a 22-residue stretch, which shows approximately 50% sequence similarity to the *Thermotoga maritima* MazG protein, which is a nucleoside triphosphate hydrolase.[4,16] Fourth, the catalytic base of the type I PRTases that generally stabilizes the N7-protonated state of the purine base to make N9 available for nucleophilic attack on the C1 carbon of PRPP[17] appears to be the β-carboxylate of the aspartate residue (Asp99) that protrudes from the PRPP binding motif of the *S. solfataricus* APRTase as in the 6-oxopurine PRTases,[4] while this catalytic function results from the γ-carboxylate from a glutamate residue located in a flexible loop in other APRTases.[9,18] Finally, the APRTase from *S. solfataricus* is active over a wide pH range with optima at pH 4.0−4.5 and around pH 8 and is strongly inhibited by ADP at low pH values.[4]

In this paper we report results of ligand binding and kinetic studies as well as four crystal structures: (1) a structure (the SsAPRT-P_i complex) refined at 2.4 Å with inorganic phosphate or sulfate bound in the 5-phosphoribosyl binding pocket, (2) an adenine bound structure (the SsAPRT-adenine complex) refined at 2.4 Å, which showed adenine together with phosphates both at the 5′-phosphoryl and PP_i positions of the presumed PRPP binding site, (3) an AMP bound structure (the SsAPRT-AMP complex) refined at 2.4 Å, and finally (4) an ADP bound structure (the SsAPRT-ADP complex), refined at 2.8 Å containing the inhibitor ADP bound like AMP with both the α- and β-phosphates occupying the 5′-phosphoribosyl binding site. No crystals of the enzyme in complex with PRPP were obtained, likely because the enzyme catalyzed a slow breakdown of PRPP to ribose 5-phosphate and PP_i.

MATERIALS AND METHODS

Materials. [8-^{14}C]-Labeled ribonucleotides and purine bases with a specific activity of 50−55 Ci/mol were bought from PerkinElmer, Sigma, or Moravec and mixed with nine parts (mol/mol) of the corresponding unlabeled compounds prior to use. [γ-^{32}P]ATP was bought from PerkinElmer NEN. The sodium salt of 5-ribosyl-α-1-phosphate (PRPP) was bought from Sigma. Buffers and precipitants for crystallization were from the *JCSG+*, *PACT* (Qiagen) and *Index* (Hampton Research) crystal screens. Other chemicals were of the highest purity available.

Determination of Adenine, AMP, ADP, and PRPP Concentrations. The concentration of PRPP in stock solutions was determined by enzyme assays as previously described.[13,19] Concentrations of adenine, AMP, and ADP were determined spectrophotometrically.

Synthesis of Radiolabeled [β-^{32}P]PRPP. [β-^{32}P]PRPP was prepared from [γ-^{32}P]ATP (3000 Ci/mmol) and ribose 5-phosphate by use of *E. coli* PRPP synthase as previously described.[13,20] Prior to use it was mixed with 1 mM unlabeled PRPP to give approximately 500 dpm/nmol. Chromatographic analyses, performed as described,[21] showed that 85−90% of the radioactivity resided in PRPP. The rest of the radioactivity was found primarily in P_i and only little (ca. 1%) in PP_i.

Purification of APRTase. *S. solfataricus* APRTase was prepared from an *E. coli* strain as previously described.[4] The extinction coefficient ε_{280} = 1.88 mL mg^{-1} cm^{-1} was calculated from the amino acid composition as described[22] and used to determine the protein concentration.

Activity Measurements. Enzyme activity was determined by measuring the conversion of [8-^{14}C]adenine (5 Ci/mol) and PRPP to [8-^{14}C]AMP and PP_i. Reactions were started by addition of PRPP to the prewarmed mixture of the other components. Samples (10 μL) were withdrawn at 1, 2, and 5 min and applied to PEI plates. Unreacted adenine was separated from the nucleotide product by chromatography in water. The radioactivity in the spots was determined by phosphorimaging using a Packard Cyclone or by liquid scintillation. A reaction without enzyme was used to determine the background (time zero) radioactivity. Most saturation curves appeared hyperbolic and the kinetic constants were calculated by fitting the reaction rates to the Michaelis−Menten equation: $v = k_{cat}[E][S]/(K_M + [S])$, but the saturation of APRTase with Mg^{2+} showed some substrate inhibition and was fitted to the equation $v = V_{max}[Mg^{2+}]/(K_M + [Mg^{2+}] \times (1 + [Mg^{2+}]/K_i))$ in which K_i denotes the inhibition constant. When the concentrations of two substrates were varied to obtain initial velocity patterns as described in Supporting Information the data were analyzed using the equation $v = V_{max}/(1 + K_{M,A}/[A] + K_{M,B}/[B] + K_{ia}K_{M,B}/([A][B]))$, in which K_{ia} denotes the

DOI: 10.1021/bi501334m
Biochemistry 2015, 54, 2323−2334

dissociation for binding of the first substrate (substrate A) to the free enzyme.

All saturation curves were analyzed using the GraphPad Prism version 5.0d for Mac OS X (GraphPad Software).

Buffers. The buffers for kinetic and ligand binding analyses were prepared at room temperature at a strength of 0.25 M. The sodium phosphate buffers were prepared by mixing 0.25 M Na_2HPO_4 with 0.25 M NaH_2PO_4 to obtain the desired pH. The phosphate/succinate buffers, used at pH values between 4.0 and 4.5, were prepared by mixing a solution of succinic acid (0.25 M) with 0.25 M NaH_2PO_4. The pH of sodium succinate buffers was adjusted by addition of NaOH and, finally, the pH of Tris-HCl buffers was adjusted by titrating a solution of Tris-base with hydrochloric acid. To determine the pH in working solutions, the buffers were diluted and $MgCl_2$ was added to give the final concentrations of buffer (50 mM) and $MgCl_2$ (0, 5, 10, or 20 mM). These solutions were then heated to the working temperature (22, 36, or 60 °C), and the resulting pH was measured.

Ligand Binding. The analyses of nucleotide and PRPP binding were carried out at 22 °C by an ultrafiltration technique using Amicon Ultrafree-MC Biomax-30 or Microcon Ultracel YM-30 centrifugal devices (Millipore) as previously described.[19,23] In short, the enzyme (5−40 μM) was mixed with the radioactively labeled ligand at concentrations up to 200 μM. The total radioactivity in the mixtures was determined in 20 μL aliquots by liquid scintillation counting. The rest of the mixtures were applied to the ultrafiltration devices, and the radioactivity in the unbound ligand was determined by counting aliquots of the liquid that had passed through the filters after a short centrifugation. In the case of [^{32}P]PRPP, which only had a purity of ∼90%, the samples were applied to PEI thin-layer plates, and following chromatography as described[21] the radioactivity in the "PRPP spot" was determined by phosphorimaging both for samples of the total mixture (unfiltered solution) and for samples of the unbound material that passed through the membrane. All binding curves appeared hyperbolic, and binding parameters were determined by fitting the data to the equation [bound ligand]/[enzyme] = [maximal binding]/[enzyme] × [free ligand]/(K_D + [free ligand]). Data were analyzed using the GraphPad Prism version 5.0d for Mac OS X (GraphPad Software).

The binding of adenine could not be accomplished by the filtration technique because of nonspecific binding of adenine to the membranes and was therefore crudely assessed by equilibrium dialysis in which only one concentration of enzyme and ligand was used per buffer type supplemented with 10 mM $MgCl_2$. The enzyme (1 mL) was dialyzed against 10 mL of 50 mM buffers containing [^{14}C]adenine with stirring for 24 h. Afterward the radioactivity of the liquid inside and outside the dialysis bag was determined by liquid scintillation and converted to adenine concentrations ($[adenine]_{inside}$ being equal to the sum of free and bound adenine and $[adenine]_{outside}$ equal to the concentration of free adenine). The specific conditions and the observed data are shown in the Supporting Table S1, Supporting Information, and the dissociation constant (K_D) was estimated by assuming one binding site per enzyme subunit using the formula: $K_D = ([enzyme] - [adenine]_{bound}) \times [adenine]_{free}/[adenine]_{bound}$, where $[adenine]_{bound} = [adenine]_{inside} - [adenine]_{outside}$.

Analysis of PRPP Breakdown. Breakdown of PRPP by APRTase (19.8 μM) was analyzed at different pH values at 36 °C. Reactions were started by addition of 100 μM [β-^{32}P]PRPP. At the indicated times samples (5 μL) were applied to PEI plates and developed in 0.85 M potassium phosphate (pH 3.4) to separate the different radioactive compounds from each other as described.[21] The radioactivity on the plates was determined by phosphorimaging, and the total radioactivity in each lane was determined as well as the radioactivity in PRPP, PP_i, and P_i "spots".

Crystallization, Data Collection, and Reduction. To determine the crystallization conditions we used the screens: *JCSG+*, *PACT* (Qiagen), and *Index* (Hampton Research). Vapor diffusion droplets were set up using an Oryx-8 crystallization robot (Douglas Instruments). All APRTase complexes were produced by cocrystallization. APRTase was easily crystallized as diffraction quality crystals were either produced directly from the screens or with little optimization. Crystallization conditions are given in Table 1. Essentially, the same hexagonal crystal form was obtained in all cases, but with varying cell dimensions. The diffraction images were recorded at the ESRF and MAXLAB synchrotrons and were indexed and integrated using XDS.[24,25] Data statistics is shown in Table 2.

Table 1. Crystallization Conditions

complex	protein and ligand concentration	buffer[a]	precipitant
SsAPRT-P_i	6.2 mg/mL	0.1 M MES (pH 6.5)	30% Jeffamine M-600
SsAPRT-AMP	14 mg/mL	0.1 M SPG (pH 4.0)[b]	25% PEG1500
	5 mM $MgCl_2$		
	2 mM AMP		
SsAPRT-ADP	14 mg/mL	0.1 M bis-TRIS (pH 5.5)	21% PEG3350
	5 mM $Mg(NO_3)_2$		0.2 M Li_2SO_4
	10 mM ATP		
SsAPRT-adenine	8.9 mg/mL	0.1 M sodium	20% PEG3350
	5 mM adenine	phosphate-citrate (pH 4.2)	0.2 M Li_2SO_4

[a]In addition, to the specified buffers the crystallization mixtures also contained components from the protein, which was dissolved in 25 mM Tris-HCl (pH 7.6) and 0.1 mM EDTA. [b]SPG, a buffer consisting of succinic acid, NaH_2PO_4 and glycine in a molar ratio of 2:7:7.

Structure Determination. A preliminary data set of APRTase, crystallized without added ligands, diffracting to 2.8 Å resolution collected at MAXLAB in Lund, Sweden, was used for molecular replacement. As search templates, structures with PDB codes 1NUL (XGPRTase from *E. coli*[26]) and 1VDM (purine phosphoribosyltransferase from *Pyrococcus horikoshii*) were used. They showed respectively 28% identity for 138/210 aligned residues and 34% identity for 148/210 aligned residues. The alignable parts (1NUL: residues 3−62 and 71−152 and 1VDM: residues 5−63 and 66−146) were superposed and side chains cut back to alanines. The resulting average structure was used as the search model for *PHASER*.[27] The self-rotation function calculated with *AMoRe*[28] indicated that it was a dimer with two subunits in the asymmetric unit. The space group possibility $P6_1$ gave a clear-cut solution in *PHASER* ($P6_5$ did not) with a translation function Z-score of 9.4 after positioning of two entities. The 1NUL and 1VDM alignable parts, correctly positioned in the unit cell, were refined separately with *CNS*,[29] now including all side chains (albeit wrong, the side chain antibumping restraints kept the model from deteriorating during initial vigorous molecular dynamics). This initial torsion

DOI: 10.1021/bi501334m
Biochemistry 2015, 54, 2323−2334

Table 2. Data Collection and Refinement Statistics of *S. solfataricus* APRTase Crystals

complex	SsAPRT-P_i	SsAPRT-AMP	SsAPRT-ADP	SsAPRT-adenine
Data				
Beamline	ID14-2 ESRF	ID14-2 ESRF	ID14-2 ESRF	I911-2 MAX-lab
$a = b$ (Å)	125.6	134.6	135.7	137.2
c (Å)	69.7	53.1	54.2	53.8
numbers of unique reflections	24681	21756	14259	22904
resolution (Å)	20−2.40	20−2.40	20−2.80	30−2.40
outer shell	(2.49−2.40)	(2.49−2.40)	(2.90−2.80)	(2.46−2.40)
R_{merge} (%)	9.3 (48.4)	9.0 (48.9)	14.5 (46.5)	6.2 (39.0)
completeness (%)	99.9 (99.9)	99.9 (99.7)	100.0 (99.9)	99.6 (100.0)
redundancy	8.4 (8.2)	7.5 (5.5)	8.6 (8.4)	13.6 (13.5)
$I/\sigma(I)$	23.8 (4.1)	21.7 (3.4)	18.3 (5.0)	28.3 (6.4)
Refinement				
R_{work}/R_{free} (%)	22.8/28.7	19.0/24.2	17.2/22.2	20.0/24.2
r.m.s. bonds	0.008	0.007	0.008	0.008
r.m.s. angles	0.985	1.060	1.151	0.982
B-factors (Å^2)				
protein	56	39	28	44
ligand	90	37	23	43
water	47	39	22	44

Table 3. Steady-State Kinetic Parameters of *S. solfataricus* APRTase at Two pH Values and 60 °C[a]

	Apparent kinetic constants for the saturation of APRTase with					
	Mg^{2+}		PRPP		adenine	
buffer[a]	K_M (μM)	k_{cat} (s^{-1})[b]	K_M (μM)	k_{cat} (s^{-1})[b]	K_M (μM)	k_{cat} (s^{-1})[b]
succinate-phosphate (pH 4.1)	3.0 ± 0.7	3.8 ± 0.5	21.9 ± 4.7	5.0 ± 0.2	10.6 ± 4.1	5.3 ± 0.3
Tris-HCl (pH 7.4)	0.47 ± 0.11[c]	8.0 ± 0.5	115 ± 6	7.2 ± 0.8	0.4 ± 2.1	5.4 ± 0.8

[a]Buffers were at 50 mM concentrations and prepared as described in Materials and Methods. The concentration of the indicated compound was varied, while the other substrates were kept at constant concentrations: PRPP at 2.6 mM, [8-^{14}C]adenine at 100 μM and $MgCl_2$ at 20 mM. [b]The three k_{cat} values obtained in the same buffer should in principle be identical. The deviation between them is probably due to experimental error, most likely uncertainty in the amount of enzyme used. [c]High concentration of Mg^{2+} inhibited the reaction with a K_i = 5.4 ± 1.5 mM determined by fitting of reaction velocities (v) to the equation: $v = V_{max} \times [Mg^{2+}]/(K_M + [Mg^{2+}] \times (1 + [Mg^{2+}]/K_i))$.

angle refinement resulted in R_{work}/R_{free} of 0.48/0.51 and 0.46/0.50, respectively, and we continued refinement with this latter model. To avoid incorrect interpretation, initial averaged $3F_{obs} - 2F_{calc}$ and $F_{obs} - F_{calc}$ maps were calculated with only backbone atoms (C_α, C, O, and N) contributing to F_{calc}. Manual rebuilding was performed with *Coot* (version 0.7)[30] using NCS (noncrystallographic symmetry) averaged $3F_{obs} - 2F_{calc}$ and $F_{obs} - F_{calc}$ maps and alternated with refinement. With that data set (25−2.8 Å resolution) 209/210 residues were modeled and refined to R_{work}/R_{free} of 0.276/0.300. The R_{free} value is based on 5% of the reflections not used for refinement.

Refinement. All four structures were refined and rebuild using *PHENIX* (version 1.5)[31] and *Coot*[30] respectively. Almost the entire sequence, residues 2−210, was modeled into the A and B chain of the dimer. At the two active sites, ligands were modeled. These symmetric parts were restrained with 2-fold noncrystallographic symmetry during refinement. The two ends of the PRPP binding site (ribose-5-phosphate at Asp99-Ser104 and PP_i at Arg40 and Lys62) were always seen occupied by phosphate (or sulfate?) groups: Either two free phosphates in the P_i complex and the adenine complex or one free phosphate at the PP_i end and the 5′-phosphate of the nucleotides in the AMP and ADP complexes. In the AMP, ADP, and adenine complexes of SsAPRTase, an additional phosphate group per dimer was modeled with ligands Glu191-Asn192 in subunit B and symmetry related Lys20 in subunit A. Finally, water molecules 66, 156, 85, and 157 were modeled for the four structures containing P_i, AMP, ADP, or adenine, respectively. Refinement statistics are given in Table 2. Figures were created using PyMOL (PyMOL Molecular Graphics System, Version 0.99 Schrödinger, LLC).

RESULTS

The APRTase from *S. solfataricus* P2 is specific for adenine and active over a wide pH range (3.5 < pH < 9.5) displaying optima both at pH values around 4 and at pH 7−8 (ref 4 and Supporting Figure S1, Supporting Information). We therefore analyzed the steady-state kinetic and ligand binding parameters both at acid and neutral pH.

Analysis of Reaction Kinetics. Table 3 shows the apparent kinetic constants obtained for the saturation of APRTase with Mg^{2+}, PRPP, and adenine at 60 °C and at pH 7.4 and at pH 4.1, when one substrate was varied at fixed concentrations of the two other substrates. The reaction requires Mg^{2+} both at pH 7.4 and at pH 4.1. The K_M for PRPP is 5-fold higher (115 ± 6 μM) in Tris-HCl at pH 7.4 than in succinate-phosphate at pH 4.1 (22 ± 5 μM). Because of this large difference in the K_M value, and since the acidic buffer contained phosphate, while the neutral buffer did not, we also determined the saturation of the enzyme with PRPP in a sodium phosphate buffer at pH 7.9. This analysis, which yielded a K_M for PRPP equal to 98 ± 13 μM, was made at 36 °C, because a substantial precipitation of magnesium phosphate

DOI: 10.1021/bi501334m
Biochemistry 2015, 54, 2323−2334

Table 4. Ligand Binding Parameters of PRPP, AMP, and ADP to *S. solfataricus* APRTase[a]

		buffers			
ligand		succinate-phosphate (pH 4.3)	succinate-phosphate without Mg^{2+} (pH 4.3)	Tris-HCl (pH 7.4)	sodium phosphate (pH 7.4)
PRPP	K_D (μM)	13 ± 4	137 ± 13[c]	0.34 ± 0.05	0.64 ± 0.08
	n[b]	0.93 ± 0.11		0.61 ± 0.02	0.58 ± 0.01
AMP	K_D (μM)	0.53 ± 0.08		142 ± 91	9.9 ± 1.0
	n[b]	0.88 ± 0.03		1.24 ± 0.56	0.63 ± 0.02
ADP	K_D (μM)	0.12 ± 0.03	0.12 ± 0.03	147 ± 6[c]	241 ± 4[c]
	n[b]	0.91 ± 0.04	0.90 ± 0.03		

[a]Binding were performed at 22 °C by the filtration technique described in Materials and Methods. The buffers were 50 mM and they contained 10 mM $MgCl_2$ unless otherwise stated. [b]Mol of ligand bound per mol subunit. [c]Calculated assuming the binding stoichiometry, n = 1.

took place at 60 °C. The apparent K_M for adenine was ca. 11 μM in the succinate-phosphate buffer at pH 4.1, but in Tris-HCl at pH 7.4 and 60 °C it did not deviate significantly from zero, when the concentration of PRPP was kept constant at 2.6 mM, which we believe is saturating for the enzyme reaction (Table 3). We also found very low values of the apparent K_M for adenine, determined in the presence of 2.6 mM PRPP at 36 °C both in Tris-HCl pH 7.5 (0.59 ± 0.48 μM) and in sodium phosphate at pH 7.9 (1.3 ± 0.6 μM). In addition, an initial velocity pattern made from 25 combinations of PRPP and adenine concentrations made in Tris-HCl at pH 7.5, 10 mM $MgCl_2$ and 60 °C (shown in the form of double reciprocal plots in the Supporting Figure S2, Supporting Information) gave the kinetic parameters $K_{M,adenine}$ = 0.0 ± 1.2 μM, K_{ia} (for adenine) = 11 ± 5 μM, $K_{M,PRPP}$ = 196 ± 52 μM, a very high, though undefined K_{ia} (for PRPP) ($7 \times 10^6 \pm 2 \times 10^{10}$ μM) and a value of V_{max} = 26.6 ± 2.3 μM min^{-1} mg^{-1} corresponding to the value k_{cat} = 10.7 ± 0.8 s^{-1}. These data all indicate that the presence of phosphate only has a marginal influence on the kinetic parameters and that the true K_M for adenine is very close to zero in neutral solution.

Ligand Binding. The binding of PRPP, AMP, and ADP was assessed by the filtration technique described in Materials and Methods, and the calculated parameters are shown in Table 4. The enzyme clearly binds 1 mol of PRPP, AMP, and ADP per mol of subunit at pH 4. The binding stoichiometry was more uncertain at neutral pH with values ranging from 0.6 to 1.2 for AMP and PRPP. Mg^{2+} strongly enhances the binding of PRPP at pH 4.5, lowering K_D from 137 ± 13 μM to 13 ± 4 μM. ADP, which is a strong inhibitor of the enzyme's activity at pH 4, but hardly inhibits at neutral pH,[4] binds tightly to the enzyme at pH 4.3 (K_D = 0.12 μM) even in the absence of Mg^{2+}, but binds only weakly at pH 7.4 (K_D = 140−240 μM). Inorganic phosphate tightened the binding of AMP considerably, reducing K_D about 10-fold at pH 7.4 (Table 4 and Supporting Figure S4), while it seemed to have a slight inhibitory effect on the binding of PRPP.

The binding of adenine could not be assessed by the filtration technique because of a strong nonspecific adhesion to the filters. Instead the binding strength was estimated by equilibrium dialysis as outlined in Materials and Methods and in the Supporting Table S1. The binding was very weak in the absence of phosphate with dissociation constants, $K_D \approx 400$ μM at pH 4.1 and $K_D \approx 250$ μM at pH 7.4, derived by assuming a binding stoichiometry, n = 1. However, adenine binds much more strongly in the presence of phosphate, K_D = 1−2 μM at pH 4.1 and $K_D \approx 30$ μM at pH 7.4, again assuming the binding stoichiometry, n = 1.

Hydrolysis of PRPP. During the ligand binding assays in which the enzyme concentration exceeded the concentration of ligand, we observed that the preparation of purified enzyme hydrolyzed [β-^{32}P]PRPP to [^{32}P]PP_i and ribose 5-phosphate. The kinetics of the reaction was analyzed under conditions where the enzyme was present at 19.8 μM, PRPP present at a concentration of 100 μM and [$MgCl_2$] = 10 mM. The reaction was slow with turnover rates, $k \approx 0.07$ min^{-1} at pH 4.4 and $k \approx 0.01$ min^{-1} at pH 8.0 at 36 °C (Supporting Figure S3). We do not know if this reaction is catalyzed by the APRTase itself or by the presence of minute amounts of another enzyme in the preparation. The reaction did not disturb the ligand binding analyses significantly, but it is likely responsible for our lack of success in generating a PRPP crystal complex.

Crystal Structure of the Monomer. The architecture of the monomer of the APRTase in complex with AMP is shown in Figure 1A. The central beta-sheet is formed by four parallel strands β2 (residues 34−39), β5 (residues 89−95), β6−7 (residues 119−128), and β8 (residues 138−143) of which residues 91−103 form the PRPP binding motif. A fifth strand β3 (residues 57−68) completes the five-stranded PRT core fold surrounded by three alpha helices α1 (residues 11−28), α2 (residues 42−53), and α3 (residues 102−115). This strand (β3) extends from the core and returns in an antiparallel manner with β4 (residues 73−79) thus forming an antiparallel β-hairpin that corresponds to the so-called flexible loop that adopts many (often nondiffracting) conformations in the type I PRTases and is expected to cover the active site during catalysis.[9,10,32,33] The C-terminal part of the *S. solfataricus* APRTase extends from the core to form a three-helix bundle consisting of α5 (residues 155−169), α6 (residues 177−188), and α7 (residues 197−207). In addition, two short parallel beta-sheets stacking the nucleobase moiety of AMP are formed by β1 (residues 6−8) and β9 (residues 148−150) and by β7 (residues 126−128) and β8 (residues 141−143) of which the β9 strand interacts directly with the purine base and constitutes the bottom of the hood structure.

The rest of the panels of Figure 1 show the *S. solfataricus* APRTase overlaid with the structures of human APRTase (Figure 1B), *E. coli* XGPRTase (Figure 1C), and *Giardia lamblia* APRTase (Figure 1D). Four features are clear: (1) The five-stranded β-sheet and the helices of the core part match more closely with the XGPRTase than with the APRTases; (2) the carboxylate group of Asp99 (Figure 1A), which is of major importance for the catalytic function of *S. solfataricus* APRTase,[4] is located in the H-bond distance (2.6 Å) from N7 of the adenine moiety of AMP and ADP as well as of free adenine. A similar carboxylate is found in all purine PRTases and shown to be involved in stabilizing the N7 protonated tautomer of the purine base.[9] This catalytic aspartate of *S. solfataricus* APRTase is positioned in the PRPP binding loop as in the *E. coli* XGPRTase [Asp92,[34] Figure 1C], while the

DOI: 10.1021/bi501334m
Biochemistry 2015, 54, 2323−2334

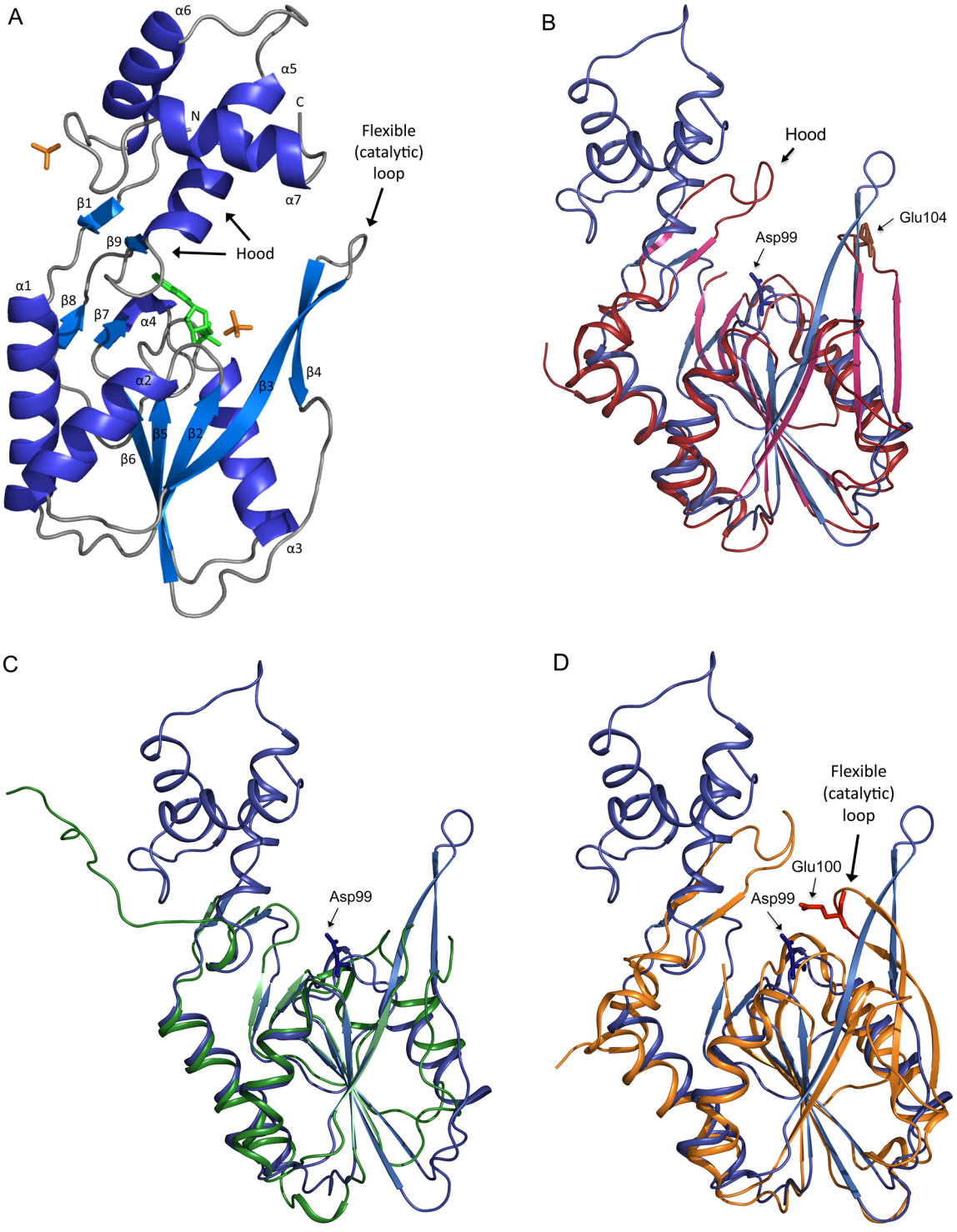

Figure 1. Structure of the monomer of *S. solfataricus* APRTase and comparison with structures of other type I PRTases. (A) structure of *S. solfataricus* APRTase subunit in complex with AMP (green) and inorganic phosphate (orange). Panels B–D, ribbon overlay of the APRTase structure with structures of other PRTases. (B) *S. solfataricus* APRTase (blue) in complex with AMP and human APRTase [red, PDB code 1ORE (44)] in complex with AMP and a chloride ion. The catalytic Asp99 (dark blue) in the *S. solfataricus* enzyme protrudes from the PRPP binding motif rather than from the flexible catalytic loop, which is the case for the catalytic important Glu104 (brown) in the human enzyme. (C) *S. solfataricus* APRTase (blue) in complex with AMP and *E. coli* XGPRTase (green, PDB code 1NUL (26) in complex with a magnesium ion and a sulfate ion. The catalytic loop of *E. coli* XGPRTase is missing from residues 61–72 in the 1NUL structure. (D) *S. solfataricus* APRTase (blue) in complex with AMP and *Giardia lamblia* APRTase (orange, PDB code 1L1R (18)) in complex with 9-deazaadenine and PRPP showing the catalytic important Glu100 (red). Note that the catalytic loop containing the catalytic Glu100 in the *G. lamblia* structure is in a loop-closed conformation, whereas all the other structures are in a loop-open conformation. Root-mean-square deviations (RMSDs) for aligned structures of *E. coli* XPRTase (1NUL), human APRTase (1ORE), and *G. lamblia* APRTase (1L1R) to the SsAPRTase core backbone atoms (residues 11–28, 34–53, 91–114, 119–128, and 138–143 of SsAPRT-AMP complex) were calculated using the PYMOL "super" command to be 0.87, 1.35 and 1.25, respectively.

DOI: 10.1021/bi501334m
Biochemistry 2015, 54, 2323–2334

corresponding catalytic carboxylate is donated by a glutamate residue located in the flexible catalytic loops of both human (Glu104, Figure 1B) and *G. lamblia* (Glu100, Figure 1D) APRTases; (3) the two β-strands (β1 and β9) in hood structure of *S. solfataricus* APRTase, which contributes to binding of the purine base, are oriented in a parallel mode and formed by residues from both the C- and the N-termini as in *E. coli* XGPRTase (Figure 1C), while the corresponding β-strands of other APRTases are antiparallel to each other and formed exclusively by residues from the N-termini of the proteins (Figure 1B,D); (4) and most striking, the hood domain is much larger in the *S. solfataricus* APRTase than in the three other enzymes (Figure 1B–D) and in type I PRTases in general.

The larger part of the hood-domain is a three-helix bundle subdomain formed by the C-terminal third of the protein, which does not match any other known protein. However, a stretch of 22 residues (152–173) shows some 50% sequence similarity to the residues 91–114 of the *Thermotoga maritima* MazG protein.[4] In all crystal structures except the P_i complex this domain has bound one molecule of inorganic phosphate (or sulfate) per dimer by contacts to Ile190, Glu191, and Asn192 in the C-terminal domain. Since the MazG protein is a nucleoside triphosphate pyrophohydrolase,[16] we considered that such an activity might also be catalyzed by the *S. solfataricus* APRTase, but our preparation of the enzyme (20 μM) left [γ-^{32}P]ATP (100 μM) untouched for half an hour at 60 °C in the presence of 10 mM $MgCl_2$ both at pH 4.3 and at pH 7.5.

Dimer and Crystal Packing. The *S. solfataricus* APRTase forms dimers in solution[4] and also in the crystals. Two separate views of the AMP bound dimer are shown in Figure 2. The flexible loop of both subunits are well structured and point away from the active sites, probably due to the $P6_1$ crystal packing forces that support interactions between residues in the loops of neighboring dimers. In this super helix, the APRTase dimers are hydrogen bonded via the β-hairpins of the flexible loop (residues Lys62-Lys79) to form four-stranded antiparallel β-sheets (Figure 3C). Interestingly, the binding of adenine, AMP, or ADP changes the unit cell's dimensions (Table 2). The *c*-axis is contracted by ca. 15 Å (from 69.7 Å in the P_i complex to ~55 Å in the SsAPRT-adenine, SsAPRT-AMP, and SsAPRT-ADP complexes), while the *a*- and *b*-axes are expanded by ca. 10 Å (from 125.6 Å in the P_i complex to ~136 Å in the SsAPRT-adenine and SsAPRT-ADP complexes). It can be understood by the $P6_1$ super helices running in the *c*-axis direction through the crystal (Figure 3) contract. We do not know whether the binding of adenine or the nucleotides are responsible for this change of crystal cell dimensions or it is due to the binding of phosphate in the C-terminal domain, since this binding of phosphate correlates with the binding of adenine compounds to the enzyme.

Ligand Binding Features. The panels of Figure 4 show crystal structures of the active site of *S. solfataricus* APRTase in complex with AMP (Figure 4A), ADP (Figure 4B), adenine (Figure 4C), and P_i (or SO_4^{2-}) alone (Figure 4D). No magnesium ion was found in the active sites of any of the complexes. However, all four structures contained phosphate or sulfate molecules (stemming from the crystallization liquids or retained during purification) in addition to the mentioned ligands. The SsAPRT-AMP complex contained one phosphate/sulfate molecule located in the PP_i binding site (Arg40, Lys62) in addition to the 5′-phosphate of the nucleotide. The SsAPRT–ADP complex contained a similarly placed phosphate/sulfate molecule in addition to the 5′-, α-, and β-phosphates, while the SsAPRT–P_i and the SsAPRT–adenine complexes both contained two phosphates: one placed like the 5′-phosphate of AMP and the other one placed in the PP_i binding site as in the AMP and ADP complexes. This phosphate is positioned as expected of the β-phosphate of PRPP in the Michaelis complex with adenine and PRPP as illustrated in Figure 5 by the overlay of ligand positions of the *S. solfataricus* APRTase–AMP complex with the 9-deazaadenine and PRPP complex of *G. lamblia* APRTase in accordance with the proposition of the electrophile migration, meaning that the ribosyl part of PRPP (C1) swings from the donor (the PP_i part of PRPP) to the accepting N atom of the nucleobase during catalysis in the PRTases.[8,18]

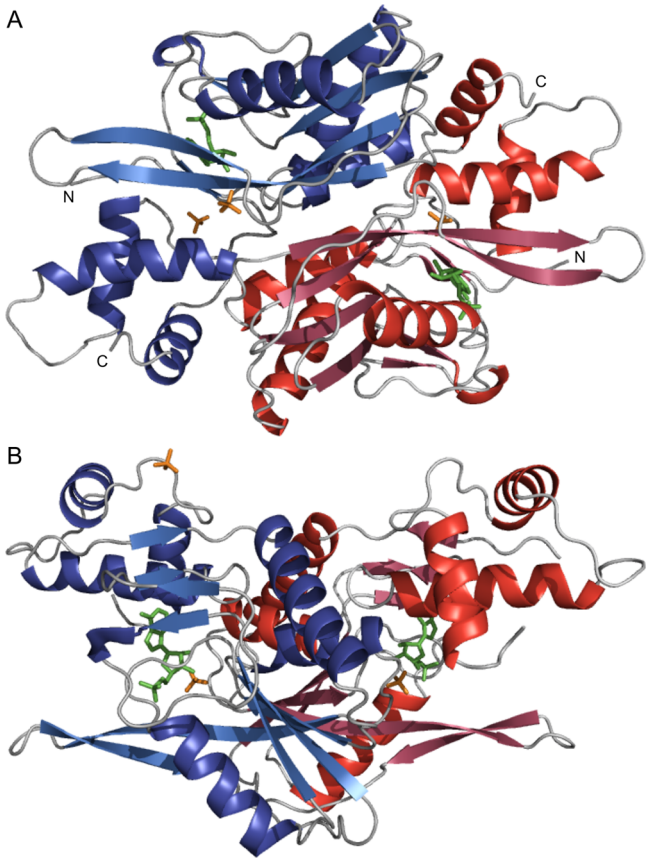

Figure 2. *S. solfataricus* APRTase dimer. Two separate views (A and B) of the AMP complex shown as a cartoon. The subunits are colored blue and red, AMP is green, and the two P_i molecules in each subunit are colored orange.

Adenine as well as the adenine moiety of the nucleotides is bound through backbone and stacking interactions from the PRTase hood structure. The amide nitrogen of Phe149 forms an H-bond to N1 of adenine (2.9–3.0 Å), and the carbonyl oxygen of Ala147 is hydrogen bonded to the N6 amino group of the purine base (2.8–3.1 Å). Furthermore, adenine stacks with the aromatic ring of Trp148 and forms an H-bond between N7 and the carboxylate group in the side chain of Asp99 (Figure 4A–C). In the AMP complex, O2′ and O3′ of the ribosyl moiety of the nucleotide are bound by H-bonds to the Asp95 (3.2 Å) and Asp96 (2.8–2.9 Å) side chains in the PRPP binding motif of the PRTase core fold. The 5′-ribosylic phosphate makes H-bonds with the backbone nitrogen atoms of Asp99 (2.8 Å), Thr100 (3.1 Å), Gly101 (2.8 Å), and Ser103

DOI: 10.1021/bi501334m
Biochemistry 2015, 54, 2323–2334

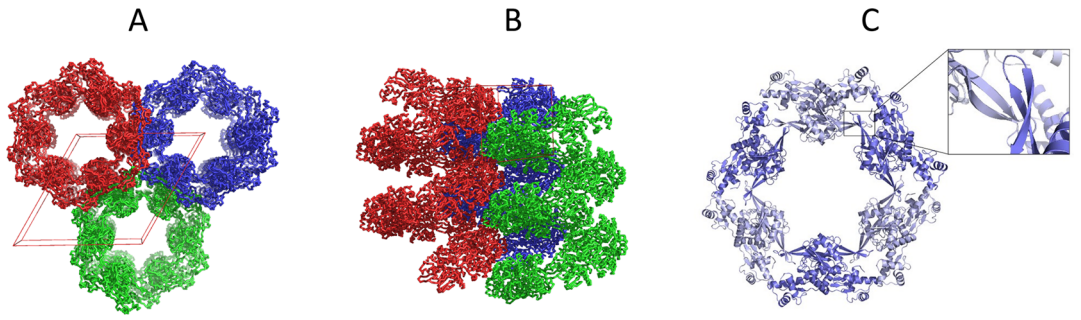

Figure 3. Crystal packing. The panels show different views of the three $P6_1$ helix with dimers interconnected by pairs of β-hairpins forming four stranded antiparallel β-sheets. (A) The helices viewed from the top, (B) is a side view, and (C) shows the interconnection by the four stranded antiparallel β-sheets.

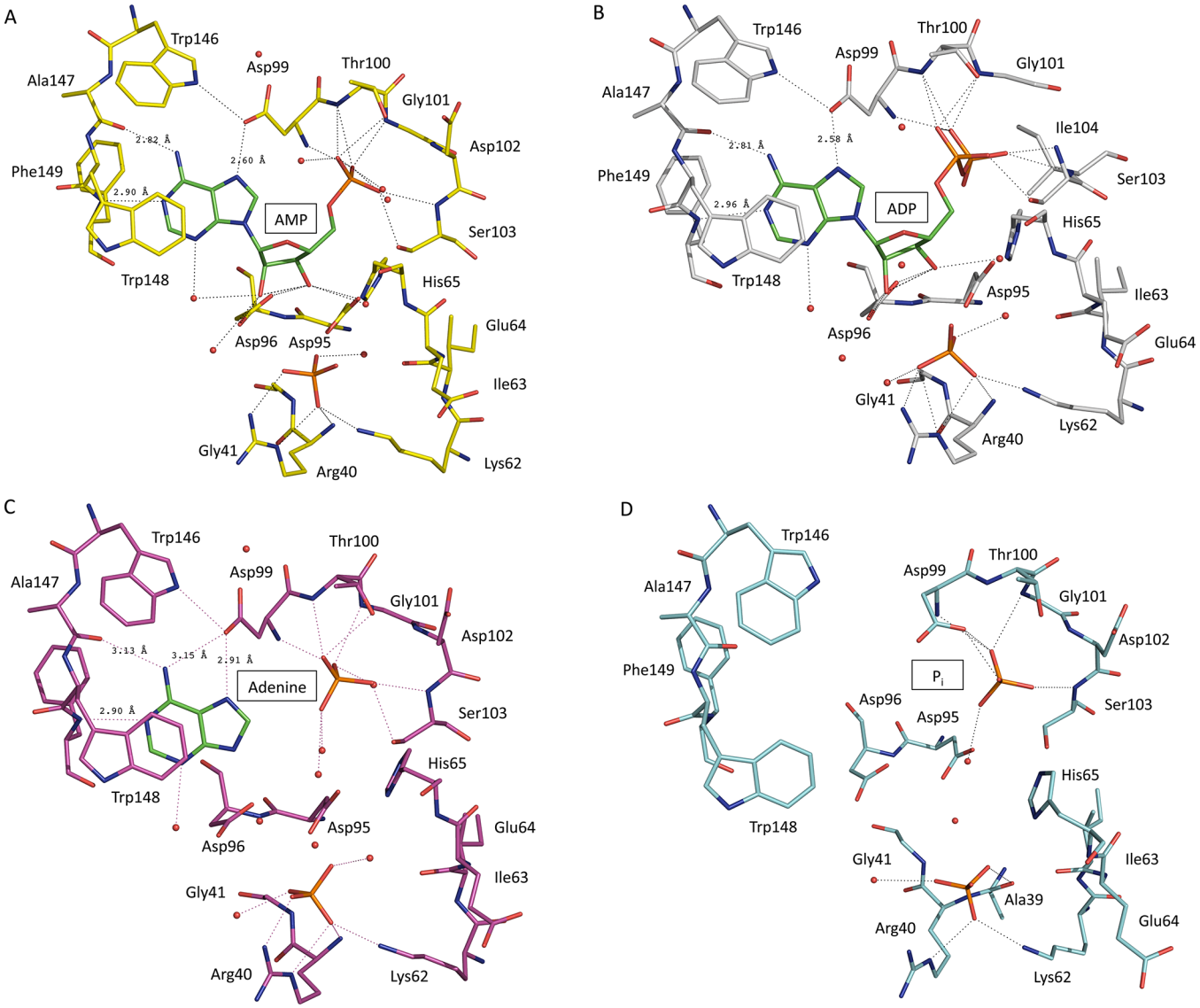

Figure 4. Depiction of the active site nucleotides and residues in the active sites of four APRTase crystal structures. Carbon atoms in the ligands are colored green. (A) The SsAPRT−AMP complex; (B) the SsAPRT−ADP complex; (C) the SsAPRT−adenine complex; and (D) the SsAPRT−P_i complex. H-bonds shorter than 3.2 Å between the nucleotides and protein residues are shown.

(3.0 Å) of the PRPP binding motif of which also the side chains of Thr100 (3.0 Å) and Ser103 (2.8 Å) participate (Figure 4A).

The inhibitor ADP binds the APRTase similarly to AMP with the β-phosphate also located the PRPP binding pocket (Figure 3B).

The binding of adenine compounds causes a contraction of the active site observed in these crystal complexes when superimposed with the P_i complex in the PRTase core fold. The contraction involves slight movement (up to 4 Å) toward active site, of strands β1 and β9 of the hood structure residues 2−8

DOI: 10.1021/bi501334m
Biochemistry 2015, 54, 2323−2334

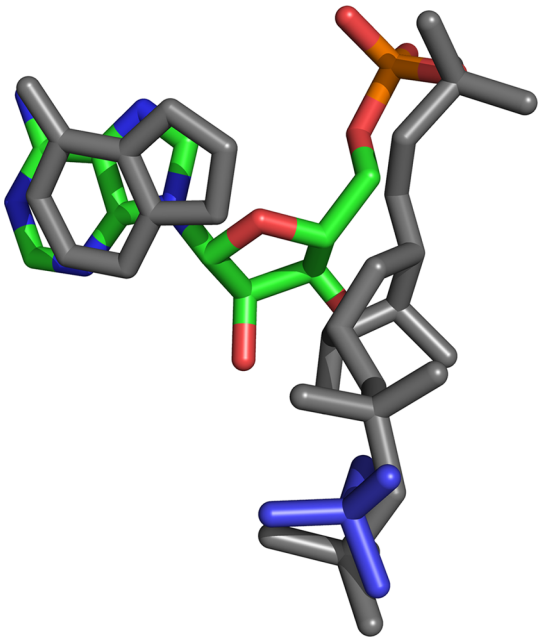

Figure 5. Overlay of ligands from the *S. solfataricus* APRTase AMP structure (green and blue) with the PRPP and 9-deazaadenine complex (gray) of *G. lamblia* [gray; PDB code 1L1R (18)].

and 144−150 as well as of the residues 165−196 of the C-terminal three-helix bundle notably the $\alpha 6$ helix. As a consequence, the carboxylate oxygen of Asp99 is within hydrogen bond distance (3.1 Å) to the heterocyclic nitrogen atom of Trp146 in the adenine-bound complexes, while this distance is 5.5 Å in the P_i complex.

DISCUSSION

The open reading frame SSO2342 in the *S. solfataricus* genome was originally annotated as a gene (*gpT-1*) encoding a 6-oxopurine PRTase, because the predicted protein shows much higher sequence similarity to known 6-oxopurine PRTases than to known APRTases.[3] However, as the purified enzyme turned out to be highly specific for adenine as the nucleobase substrate exhibiting extremely low activity with the 6-oxopurine bases, we suggested that the gene should be renamed *apt*.[4]

In many ways, the *S. solfataricus* enzyme is an unusual APRTase. The first feature is the nature of the catalytic carboxylate that functions to stabilize the N7 protonated tautomer of the purine base substrate and thus setting N9 free for nucleophilic attack on the C1 of PRPP in all purine PRTases.[9] In the *S. solfataricus* APRTase, this function is carried out by the β-carboxylate group of Asp99, which we find protruding from the PRPP binding motif as in the 6-oxopurine PRTases, and located within hydrogen bonding distance (2.6 Å in the SsAPRT-AMP and SsAPRT-ADP complexes and 3.1 Å in the SsAPRT-adenine complex) from the N7 position of the adenine base in all crystal complexes (Figure 4). In other characterized APRTases this catalytic carboxylate is provided by a glutamate residue present in the flexible loop and observed within hydrogen bonding distance to N7 of adenine in closed active site structures (Figure 1B). The major specificity determinants in the active site of the *S. solfataricus* APRTase that make the enzyme discriminate against the 6-oxopurine bases and prefer adenine as the substrate are likely the H-bond between the amide nitrogen of Phe149 and N1 of adenine, and the H-bond between the carbonyl oxygen of Ala147 and the N6 amino group of the purine base. Such H-bonds cannot form with the 6-oxopurines, because they have a keto-group in the 6-position and because N1 of the base is protonated and thus only able to act as H-bond donor.

Another feature of the structure of the *S. solfataricus* APRTase is that the 3-helical domain, formed by C-terminal third of the polypeptide chain, has no counterpart in any other characterized PRTases and is without sequence similarity to any known protein except the small stretch of 22 residues (152−173) where it shows a weak sequence similarity to the MazG protein of *Thermotoga maritima* (PDB code 2YXH). In the *S. solfataricus* APRTase, this 3-helical bundle domain is "inserted" in the hood of the enzyme, making the hood domain considerably larger than in other PRTases. The function of this domain is unclear, but it contributes indirectly to nucleobase binding and stabilization of the dimer.

Specificity Determinants and Catalytic Properties. The APRTase binds the substrate PRPP, the product AMP, and the inhibitor ADP in the active site at a 1:1 stoichiometry (Table 4). The binding of PRPP required Mg^{2+}, while the binding of ADP, which was strong at pH 4, but weak at neutral pH, took place without the participation of Mg^{2+}. The enzyme's affinity for adenine was weak in phosphate-free buffers ($K_D \approx 200\ \mu M$), but strongly enhanced in the presence of phosphate ($K_D = 1-2\ \mu M$ at pH 4.1). Likewise, the binding of AMP was tightened 10−15-fold by phosphate (Table 4 and Supporting Figure S4), which had marginal inhibitory effect on the binding of PRPP. This indicates that phosphates organize and adjust the active site cavity for adenine and adenine nucleotide binding resulting in a tighter binding of the base/nucleotide. The adenine and the P_i complexes contained two phosphates (or sulfates). One of these is positioned as the 5′-phosphate of AMP; the other is positioned in the PP_i binding site, where the β-phosphate of PRPP is situated in the catalytic loop-closed Michaelis complex of APRTase from *G. lamblia*[18] as illustrated in Figure 5, which is an overlay of ligand positions in the *S. solfataricus* APRTase complex and the 9-deazaadenine and PRPP complex of *G. lamblia* APRTase. This is in accordance with the general mechanism of electrophile migration, meaning that the electrophilic C1-end of the ribosyl part of PRPP swings away from the pyrophosphoryl group up to the nucleophilic nitrogen of the nucleobase base during catalysis as seen in PRTase−substrate complexes and documented by studies of isotope effects on the reaction kinetics.[9,18,35,36] There is an apparent conflict between our kinetic analysis of the enzyme and the results of our ligand binding analyses. The initial velocity pattern, shown in the Supporting Figure S2, and the kinetic parameters in Table 3, indicate that K_M for adenine at neutral pH, does not deviate significantly from zero ($K_M = 0.0 \pm 1.2\ \mu M$) and that the binding of PRPP to the free enzyme is negligible at pH 7.5. These results are best explained by an ordered, equilibrium reaction mechanism with adenine binding first to the free enzyme. For such mechanisms, the K_M for substrate A is zero, because at saturating (i.e., infinitely high) concentration of the second substrate (B) the substrate A will be pulled into the ternary, catalytically active (EAB) complex immediately after binding to the enzyme no matter how low the concentration of substrate A is.[37] The APRTase of *S. sulfolobus* may act by such a kinetic mechanism, but this interpretation is not easily reconciled with the results of the ligand-binding analyses, which showed strong binding of PRPP to the free enzyme and only poor binding of adenine (at least in

DOI: 10.1021/bi501334m
Biochemistry 2015, 54, 2323−2334

phosphate-free buffers). In addition, such a mechanism deviates from the general trend that PRTases bind PRPP prior to the nucleobase or exhibit a random binding order with predominant binding of PRPP as the first substrate, see, e.g. references 9, 15, 19, and 38. The binding of PRPP to *S. solfataricus* APRTase was strong, and it is easy to imagine that the binding of PRPP to the free enzyme may structure the active site cavity in the same way as the phosphates do in the crystal structure of the SsAPRTase−adenine complex (Figure 4C) and thus promote strong binding of adenine to the enzyme−PRPP complex. Thus, the substrate binding parameters suggest that the APRTase of *S. solfataricus* obeys a sequential reaction mechanism with PRPP binding first to the enzyme resulting in a strong subsequent binding and a low K_M for adenine, perhaps with an alternative branch involving binding of adenine prior to PRPP in the presence of inorganic phosphate. The binding analyses were carried out at room temperature (~22 °C), while the kinetics were analyzed at 60 °C. This difference in temperature is likely to cause some change in the enzyme's affinity for the substrates, but it seems unlikely that the affinity for PRPP would change from the strong affinity ($K_D \leq 1$ μM) seen at 22 °C to virtually no binding at 60 °C as indicated by the kinetics. It is also difficult to understand how an equilibrium mechanism with a K_M for adenine at pH 7.5 can shift to a mechanism with a defined K_M for adenine (different from zero, Table 3), when the pH is reduced to 4.1 (Table 3). More experiments are clearly needed to resolve the reaction mechanism(s) at the two pH optima. We do not know if the stimulation of the binding of adenine (and AMP) by 50 mM phosphate has any relevance *in vivo*. As far as we know, the intracellular concentration of inorganic phosphate has never been determined for any *Sulfolobus* species, but it may be 5−20 mM as for other organisms, for example, *Saccharomyces cerevisiae*.[39]

Structural Changes Observed in APRTase. Upon comparison of the nucleobase and nucleotide bound crystal complexes and the P_i complex (Figure 4), it appears that Asp99 of APRTase plays two different roles. In the three complexes with adenine compounds, Asp99 participates in an H-bond network between Trp146 of the hood, which also contacts adenine through backbone interactions and stacking from Trp148, and N7 and the N6 amide of the adenine moiety. In the P_i complex (Figure 4D), the side chain of Asp99 is directed toward the phosphate in the PRPP binding pocket that corresponds to the 5′-phosphate of the AMP structure (Figure 4A). In addition residues of the hood-structure (residues 144−150), the N-terminal (residues 2−8) and the α6 helix of the C-terminal domain (residues 165−196) are found dislocated approximately 1.5 Å away from the active site. This finding suggests that nucleobase or nucleotide binding is followed by a structural change in APRTase, which allows Asp99 to form an H-bond (3.0−3.1 Å) to the nitrogen atom of the indolyl ring of Trp146 as seen in the complexes containing adenine, AMP, or ADP, while these two atoms are 5.5 Å away from each other in the SsAPRT−P_i complex.

The hairpin structure of *S. solfataricus* APRTase, which is formed by the antiparallel hairpin β3 and β4 and corresponds to the flexible loop of other type I PRTases,[9,10,32,33] adopts the same conformation in all resolved structures, regardless the bound ligand. We ascribe this apparent lack of flexibility to the $P6_1$ crystal lattice that favors interaction between neighboring dimers, as shown in Figure 2C.

Binding of ADP. The binding of ADP to SsAPRTase was a fortuitous finding. We tested if addition of the four common nucleoside triphosphates would influence the activity of the enzyme, because of earlier findings that CTP inhibits and GTP activates the uracil PRTase of *S. solfataricus*.[23,40,41] These tests revealed a moderate inhibitory effect of ATP, and therefore ATP was added to the crystallization mixtures. However, when the crystal structure was solved it appeared that ADP, not ATP, was bound in the active site of the enzyme as shown in Figure 4B. Subsequent analyses showed that ADP was an almost 20-times stronger inhibitor of *S. solfataricus* APRTase activity than ATP, and also a much stronger inhibitor than AMP but interestingly only in acid solution (pH 4−5). At neutral pH it was at best a very weak inhibitor.[4] In the crystal structure, ADP binds similarly to AMP, but with the additional β-phosphate located deeper inside the PRPP binding pocket. We are currently not able to propose a physiological meaning of this inhibition by ADP. Although *S. solfataricus* is a thermoacidophile organism with optimal growth at pH 2−4, the pH in the cytoplasm is believed to be neutral.[3] The binding of ADP was independent of Mg^{2+} at acid pH, while the binding at neutral pH was very weak even in the presence of Mg^{2+} (Table 4). This may be because the 5′-diphosphate moiety only has little negative charge at pH 4, while it is more strongly charged at pH 7−8. The crystal structure (Figure 4B) reveals that there are no positive charges, but an H-bond network surrounding the 5′-phosphates in the enzyme and perhaps, there is too little space in the enzyme to accommodate the Mg ion, which binds strongly to the 5′-diphosphate of ADP at neutral pH.[42] In any case, to our knowledge this is the first observation of a nucleoside diphosphate bound to a PRTase, but for the structurally and functionally related PRPP synthetase, ADP binds both in the active site as a competitive inhibitor against ATP and as an allosteric inhibitor in a second site.[43]

APRTases of other Crenarchaeota. Genes encoding APRTase have not been identified in any species of the Crenarchaeotae branch, probably because of the higher sequence similarity of the encoding genes to the 6-oxopurine PRTases than to any previously characterized APRTases. We therefore anticipate that all open reading frames of the Crenarchaeotae with major sequence similarity to the open reading frame SSO2342 of *S. solfataricus* encode the APRTase of the organism and propose that the genes should be renamed *apt*.

The pH−Activity Profile. The APRTase from *S. solfataricus* is active over a wide pH range, 3.5 ≤ pH ≤ 10, showing peaks of activity near pH 4.5 and pH 8, and the activity is lost (or very strongly reduced) both in acid and in neutral solution by mutational change of Asp99 to asparagine.[4] Our current results do not explain how the enzyme can function equally well at pH 4 and pH 8. Many things can change as functions of pH, for example: Complex mutual titration of side chain residues (e.g., Arg40, Glu64, His65, Lys62, Asp95, Asp96, Asp99, or Asp102) together with titration of the substrate molecules may underlie the broad pH activity profile and the decline in activity around pH 5.5. We also found some activity of *E. coli* APRTase at pH 4,[4] but as far as we know the activities of PRTases have generally not been studied at this low pH.

Breakdown of PRPP. We did not obtain enzyme complexes with PRPP likely because the protein preparations broke down PRPP to PP_i and ribose 5-phosphate. The breakdown was faster at low pH but still much slower than the PRTase reaction. It may be due to a minor contamination

DOI: 10.1021/bi501334m
Biochemistry 2015, 54, 2323−2334

of the preparation with a foreign enzyme. However, as we do not know of any such enzyme in *E. coli*, and since most *E. coli* proteins denature during heating at 74 °C, which was used during purification of the *Sulfolobus* enzyme,[4] we tend to believe that APRTase itself is responsible for the reaction, a notion that is supported by the finding that ATP (100 μM) remained stable when incubated with the enzyme (20 μM) half an hour at 60 °C. A slow breakdown of PRPP to PP_i and ribose 5-phosphate was observed for some other PRTases[40,41] and interpreted as a side reaction resulting from a nucleophilic attack of water on the C1 of PRPP in the active site of the enzymes in the absence of a functional nucleobase. The hydrolysis of PRPP by *S. solfataricus* APRTase may similarly be catalyzed by the active PRTase site or alternatively by the C-terminal domain of unknown function.

■ ASSOCIATED CONTENT

Supporting Information

(1) The primary data underlying the determination of the strength of adenine binding by equilibrium dialysis (Table S1). (2) An autoradiogram demonstrating the separation of adenine and AMP by chromatography on PEI-plates and the two reaction optima of *S. solfataricus* APRTase at pH 4 and pH 7−8 (Figure S1). (3) Double reciprocal plots of reaction velocities at 25 different concentrations of PRPP and adenine. (4) A figure showing the kinetics of PRPP-breakdown at two different pH values (Figure S3). (5) Binding curves for adenine in phosphate-containing and phosphate-free buffers. The Supporting Information material is available free of charge via the Internet at http://pubs.acs.org.

Accession Codes

The SsAPRT−P_i complex, a crystal structure of *S. solfataricus* APRTase without adenine compounds, but containing P_i or sulfate (PDB code 4TRB); the SsAPRT−adenine complex, a crystal structure of *S. solfataricus* APRTase in complex with adenine and P_i (PDB code 4TRC); the SsAPRT−AMP complex, a crystal structure of *S. solfataricus* APRTase in complex with AMP and P_i or sulfate (PDB code 4TS5); the SsAPRT−ADP complex, crystal structure of *S. solfataricus* APRTase in complex with ADP and P_i or sulfate (PDB code 4TS7).

■ AUTHOR INFORMATION

Corresponding Authors

*(K.F.J.) E-mail: kajfrankjensen@gmail.com.
*(A.K.) E-mail: kadziola@chem.ku.dk.

Present Address

#(K.S.J.) Lund University, Department of Biophysical Chemistry, Center for Molecular Protein Science, P.O. Box 124, SE-221 00 Lund, Sweden.

Funding

Det Frie Forskningsråd, Natur og Univers.

Notes

The authors declare no competing financial interest.

■ ACKNOWLEDGMENTS

We thank Lise Schack for excellent technical assistance and the staff at ESRF ID14 and MAX IV I911-2 crystallography beamlines for excellent help and support provided during the experiments.

■ ABBREVIATIONS

PRTase, phosphoribosyltransferase; APRTase, adenine PRTase; XGPRTase, xanthine-guanine PRTase; AMP, adenosine monophosphate; ADP, adenosine 5′-diphosphate; PRPP, 5-phosphoribosyl-α-1-pyrophosphate; P_i, inorganic phosphate; PP_i, pyrophosphate; MES, 2-(*N*-morpholino)ethanesulfonic acid; bis-TRIS, 2,2-bis(hydroxymethyl)-2,2′,2″-nitrilotriethanol; PEI-plates, polyethylenimine impregnated cellulose thin-layer plates on plastic sheets.

■ REFERENCES

(1) Jensen, K. F. (1983) Metabolism of 5-phosphoribosyl 1-pyrophosphate (PRPP) in *Escherichia coli* and *Salmonella typhimurium*, in *Metabolism of Nucleotides, Nucleosides and Nucleobases in Microorganisms* (Munch-Petersen, A., Ed.) pp 1−25, Academic Press, London.

(2) Jensen, K. F., Dandanell, G., Hove-Jensen, B., and Willemoës, M. (2008) in *EcoSal—Escherichia coli and Salmonella: Cellular and Molecular Biology* (Böck, A., Curtiss, R., III, Kaper, J. B., Karp, P. D., Neidhardt, F. C., Nyström, T., Slauch, J. M., and Squires, C. L., Eds.) ASM Press, Washington, D.C., http://www.ecosal.org.

(3) She, Q., Singh, R. K., Confalonieri, F., Zivanovic, Y., Allard, G., Awayez, M. J., Chan-Weiher, C. C., Clausen, I. G., Curtis, B. A., De Moors, A., Erauso, G., Fletcher, C., Gordon, P. M., Heikamp-de Jong, I., Jeffries, A. C., Kozera, C. J., Medina, N., Peng, X., Thi-Ngoc, H. P., Redder, P., Schenk, M. E., Theriault, C., Tolstrup, N., Charlebois, R. L., Doolittle, W. F., Duguet, M., Gaasterland, T., Garrett, R. A., Ragan, M. A., Sensen, C. W., and Van der Oost, J. (2001) The complete genome of the crenarchaeon *Sulfolobus solfataricus* P2. *Proc. Natl. Acad. Sci. U.S.A. 98*, 7835−7840.

(4) Hansen, M. R., Jensen, K. S., Rasmussen, M. S., Christoffersen, S., Kadziola, A., and Jensen, K. F. (2014) Specificities and pH profiles of adenine and hypoxanthine-guanine-xanthine phosphoribosyltransferases (nucleotide synthases) of the thermoacidophile archaeon *Sulfolobus solfataricus*. *Extremophiles 18*, 179−187 DOI: 10.100/s00798-013-0585-8.

(5) Hansen, M. R., Jensen, K. S., Rasmussen, M. S., Christoffersen, S., Kadziola, A., and Jensen, K. F. (2014) Erratum to: Specificities and pH profiles of adenine and hypoxanthine-guanine-xanthine phosphoribosyltransferases (nucleotide synthases) of the thermoacidophile archaeon *Sulfolobus solfataricus*. *Extremophiles 18*, 189 DOI: 10.1007/s00792-013-0598-5.

(6) Eads, J. C., Scapin, G., Xu, Y., Grubmeyer, C., and Sacchettini, J. C. (1994) The crystal structure of human hypoxanthine-guanine phosphoribosyltransferase with bound GMP. *Cell 78*, 325−334.

(7) Grubmeyer, C., and Wang, G. (1998) Making a nucleotide: structure and function of orotate phosphoribosyltransferase. *Paths Pyrimidines 6* (1), 1−11.

(8) Scapin, G., Grubmeyer, C., and Sacchettini, J. C. (1994) Crystal structure of orotate phosphoribosyltransferase. *Biochemistry 33*, 1287−1294.

(9) Schramm, V. L., and Grubmeyer, C. T. (2004) Phosphoribosyltransferase mechanisms and roles in nucleic acid metabolism, in *Progress in Nucleic Acids Research and Molecular Biology* (Moldave, K., Ed.) pp 261−304, Academic Press, New York.

(10) Sinha, S. C., and Smith, J. L. (2001) The PRT protein family. *Curr. Opin. Struct. Biol. 11*, 733−739.

(11) Hove-Jensen, B. (1985) Cloning and characterization of the *prs* gene encoding phosphoribosylpyrophosphate synthetase of *Escherichia coli*. *Mol. Gen. Genet. 201*, 5487−5493.

(12) Hershey, H. V., and Taylor, M. W. (1986) Nucleotide sequence and deduced amino acid sequence of *Escherichia coli* adenine phosphoribosyltransferase and comparison with other analogous enzymes. *Gene 43*, 287−293.

(13) Hansen, M. R., Barr, E. W., Jensen, K. F., Willemoës, M., Grubmeyer, C. T., and Winther, J. R. (2014) Catalytic site interactions in yeast OMP synthase. *Arch. Biochem. Biophys. 542*, 28−38.

DOI: 10.1021/bi501334m
Biochemistry 2015, 54, 2323−2334

(14) Hove-Jensen, B., Harlow, K. V., King, C. J., and Switzer, R. L. (1986) Phosphoribosylpyrophosphate synthetase of *Escherichia coli*. Properties of the purified enzyme and primary structure of the *prs* gene. *J. Biol. Chem. 261*, 6765−6771.
(15) Lundegaard, C., and Jensen, K. F. (1999) Kinetic mechanism of uracil phosphoribosyltransferase from *Escherichia coli* and catalytic importance of the conserved proline in the PRPP binding site. *Biochemistry 38*, 3327−3334.
(16) Zhang, J., Zhang, Y., and Inouye, M. (2002) *Thermotoga maritima* MazG protein has both nucleoside triphosphate pyrophosphohydrolase and pyrophosphatase activities. *J. Biol. Chem. 278*, 21408−21414.
(17) Xu, Y., and Grubmeyer, C. (1998) Catalysis in human hypoxanthine-guanine phosphoribosyltransferase: Asp 137 acts as a general acid/base. *Biochemistry 37*, 4114−4124.
(18) Shi, W., Sarver, A. E., Wang, C. C., Tanaka, K. S., Almo, S. C., and Schramm, V. L. (2002) Closed site complexes of adenine phosphoribosyltransferase from *Giardia lamblia* reveal a mechanism of ribosyl migration. *J. Biol. Chem. 277*, 39981−39988.
(19) Arent, S., Kadziola, A., Larsen, L., Neuhard, J., and Jensen, K. F. (2006) The extraordinary specificity of xanthine phosphoribosyltransferase from *Bacillus subtilis* elucidated by reaction kinetics, ligand binding, and crystallography. *Biochemistry 45*, 6615−6627.
(20) Jensen, K. F., and Mygind, B. (1996) Different oligimeric states are involved in the allosteric behavior of uracil phosphoribosyltransferase from *Escherichia coli*. *Eur. J. Biochem. 240*, 637−645.
(21) Jensen, K. F., Houlberg, U., and Nygaard, P. (1979) Thin-layer chromatographic methods to isolate ^{32}P-labeled 5-phosphoribosyl-a-1-pyrophosphate (PRPP): determination of cellular PRPP pools and assay of PRPP synthetase activity. *Anal. Biochem. 98*, 254−263.
(22) Gill, S. C., and von Hippel, P. H. (1989) Calculation of protein extinction coefficients from amino acid sequence data. *Anal. Biochem. 182*, 319−326.
(23) Arent, S., Harris, P., Jensen, K. F., and Larsen, S. (2005) Allosteric regulation and communication between subunits in uracil phosphoribosyltransferase from *Sulfolobus solfataricus*. *Biochemistry 44*, 883−892.
(24) Kabasch, W. (2010) XDS. *Acta Crystallogr., Sect. D Biol. Crystallogr. 66* (Pt 2), 125−132.
(25) Kabasch, W. (2010) Integration, scaling, space-group assignment and post-refinement. *Acta Crystallogr., Sect. D Biol. Crystallogr. 66* (Pt 2), 133−144.
(26) Vos, S., de Jersey, J., and Martin, J. L. (1997) Crystal structure of *Escherichia coli* xanthine phosphoribosyltransferase. *Biochemistry 36*, 4125−4134.
(27) McCoy, A. J., Grosse-Kunstleve, R. W., Adams, P. D., Winn, M. D., Storoni, L. C., and Read, R. J. (2007) Phaser crystallographic software. *J. Appl. Crystallogr. 40*, 658−674.
(28) Navaza, J. (1994) AMORE: an automated package for molecular replacement. *Acta Crystallogr., Sect. A 50*, 157−163.
(29) Brünger, A. T., Adams, P. D., Glore, G. M., DeLano, W. L., Gros, P., Grosse-Kunstleve, R. W., Jiang, J. S., Kuszewski, J., Nilges, M., Pannu, N. S., Read, R. J., Rice, L. M., Simonson, T., and Warren, G. L. (1998) Crystallography & NMR system: A new software suite for macromolecular structure determination. *Acta Crystallogr., Sect. D Biol. Crystallogr. 54*, 905−921.
(30) Emsley, P., and Cowtan, K. D. (2004) Coot: model-building tools for molecular graphics. *Acta Crystallogr., Sect. D Biol. Crystallogr. 60*, 2126−2132.
(31) Adams, P. D., Afronine, P. V., Bunkóczi, G., Chen, V. B., Davis, I. W., Echols, N., Headd, J. J., Hung, L. W., Kapral, G. J., Grosse-Kunstleve, R. W., McCoy, A. J., Moriarty, N. W., Oeffner, R., Read, R. J., Richardson, D. C., Richardson, J. S., Terwilliger, T. C., and Zwart, P. H. (2010) PHENIX: a comprehensive Python-based system for macromolecular structure solution. *Acta Crystallogr., Sect. D Biol. Crystallogr. 66*, 213−221.
(32) Wang, G. P., Hansen, M. R., and Grubmeyer, C. (2012) Loop residues and catalysis in OMP synthase. *Biochemistry 51*, 4406−4415.
(33) Grubmeyer, C., Hansen, M. R., Fedorov, A. A., and Almo, S. C. (2012) Structure of Salmonella typhimurium OMP synthase in a complete substrate complex. *Biochemistry 51*, 4397−4405.
(34) Vos, S., Parry, R. J., Burns, M. R., de Jersey, J., and Martin, J. L. (1998) Structures of free and complexed forms of Escherichia coli xanthine-guanine phosphoribosyltransferase. *J. Mol. Biol. 282*, 875−889.
(35) Deng, H., Callender, R., Schramm, V. L., and Grubmeyer, C. (2010) Pyrophosphate activation in hypoxanthine-guanine phosphoribosyltransferase with transition state analogue. *Biochemistry 49*, 2705−2714.
(36) Scapin, G., Ozturk, D. H., Grubmeyer, C., and Sacchettini, J. C. (1995) The crystal structure of orotate phosphoribosyltransferase complexed with orotate and alpha-D-5-phosphoribosyl-1-pyrophosphate. *Biochemistry 34*, 10744−10754.
(37) Cleland, W. W. (1963) The kinetics of enzyme-catalyzed reactions with two or more substrates or products. I. Nomenclature and rate equations. *Biochim. Biophys. Acta 67*, 104−137.
(38) Wang, G., Lundegaard, C., Jensen, K. F., and Grubmeyer, C. (1999) Kinetic mechanism of OMP synthase: A slow physical step following group transfer limits catalytic rate. *Biochemistry 38*, 275−283.
(39) Auesukaree, C., Homma, T., Tochio, H., Shirakawa, M., Kaneko, Y., and Harashima, S. (2004) Intracellular phosphate serves as a signal for the regulation of the *PHO* pathway in *Saccharomyces cerevisiae*. *J. Biol. Chem. 279*, 17289−17294.
(40) Christoffersen, S., Kadziola, A., Johansson, E., Rasmussen, M., Willemoës, M., and Jensen, K. F. (2009) Structural and kinetic studies of the allosteric transition in *Sulfolobus solfataricus* uracil phosphoribosyltransferase: Permanent activation by engineering the C-terminus. *J. Mol. Biol. 393*, 464−477.
(41) Jensen, K. F., Arent, S., Larsen, S., and Schack, L. (2005) Allosteric properties of the GTP activated and CTP inhibited uracil phosphoribosyltransferase from the thermo-acidophilic archaeon *Sulfolobus solfataricus*. *FEBS J. 272*, 1440−1453.
(42) O'Sullivan, W., and J. Smithers, G. W. (1979) Stability constants for biologically important metal-ligand complexes. *Methods Enzymol. 63*, 294−336.
(43) Gibson, K. J., Schubert, K. R., and Switzer, R. L. (1982) Binding of the substrates and the allosteric inhibitor adenosine 5′-diphosphate to phosphoribosylpyrophosphate synthetase from *Salmonella typhimurium*. *J. Biol. Chem. 257*, 2391−2396.
(44) Silva, M., Silva, C. H., Iulek, J., and Thiemann, O. H. (2004) Three-dimensional structure of human adenine phosphoribosyltransferase and its relation to DHA-urolithiasis. *Biochemistry 43*, 7663−7671.

DOI: 10.1021/bi501334m
Biochemistry 2015, 54, 2323−2334